

Optical spectroscopy study of damage evolution in 6H-SiC by H_2^+ implantation

Yong Wang(王勇), Qing Liao(廖庆), Ming Liu(刘茗), Peng-Fei Zheng(郑鹏飞), Xinyu Gao(高新宇), Zheng Jia (贾政), Shuai Xu(徐帅), Bing-Sheng Li(李[4]

Citation: Chin. Phys. B, 2021, 30 (**5**): 056106. DOI: 10.1088/1674-1056/abe9a7

Journal homepage: http://cpb.iphy.ac.cn; http://iopscience.iop.org/cpb

What follows is a list of articles you may be interested in

Degradation of β-Ga_2O_3 Schottky barrier diode underswift heavy ion irradiation

Wen-Si Ai(艾文思), Jie Liu(刘杰), Qian Feng(冯倩), Peng-Fei Zhai(翟鹏飞), Pei-Pei Hu(胡培培), Jian Zeng(曾健), Sheng-Xia Zhang(张胜霞), Zong-Zhen Li(李宗臻), Li Liu(刘丽), Xiao-Yu Yan(闫晓宇), You-Mei Sun(孙友梅)

Chin. Phys. B, 2021, 30 (**5**): 056110. DOI: 10.1088/1674-1056/abf107

Effect of tellurium (Te^{4+}) irradiation on microstructure and associated irradiation-induced hardening

Hefei Huang(黄鹤飞), Jizhao Liu(刘继召), Guanhong Lei(雷冠虹), Ondrej Muránsky, Tao Wei, Mihail Ionescu

Chin. Phys. B, 2021, 30 (**5**): 056108. DOI: 10.1088/1674-1056/abf039

Evolution of ion-irradiated point defect concentration by cluster dynamics simulation

Shuaishuai Feng(冯帅帅)[1,4], Shasha Lv(吕沙沙)[2], Liang Chen(陈良)[3], Zhengcao Li(李正操)[4]

Chin. Phys. B, 2021, 30 (**5**): 056105. DOI: 10.1088/1674-1056/abf102

Structure and luminescence of α-plane GaN on γ-plane sapphire substrate modified by Si implantation

Lijie Huang(黄黎杰), Lin Li(李琳), Zhen Shang(尚震), Mao Wang(王茂), Junjie Kang(康俊杰), Wei Luo(罗巍), Zhiwen Liang(梁智文), Slawomir Prucnal, Ulrich Kentsch, Yanda Ji(吉彦达), Fabi Zhang(张法碧), Qi Wang(王琦), Ye Yuan(袁冶), Qian Sun(孙钱), Shengqiang Zhou(周生强), Xinqiang Wang(王新强)

Chin. Phys. B, 2021, 30 (**5**): 056104. DOI: 10.1088/1674-1056/abd76a

Water and nutrient recovery from urine: A lead up trail using nano-structured In_2S_3 photo electrodes

R Jayakrishnan, T R Sreerev, Adith Varma

Chin. Phys. B, 2021, 30 (**5**): 056103. DOI: 10.1088/1674-1056/abd169

SPECIAL TOPIC — Ion beam modification of materials and applications

Optical spectroscopy study of damage evolution in 6H-SiC by H_2^+ implantation*

Yong Wang(王勇)[1], Qing Liao(廖庆)[2], Ming Liu(刘茗)[3], Peng-Fei Zheng(郑鹏飞)[3], Xinyu Gao(高新宇)[1], Zheng Jia (贾政)[1], Shuai Xu(徐帅)[2], and Bing-Sheng Li(李炳生)[2,4,†]

[1] China Institute for Radiation Protection, Taiyuan 030006, China
[2] State Key Laboratory for Environment-Friendly Energy Materials, Southwest University of Science and Technology, Mianyang 621010, China
[3] Southwestern Institute of Physics, Chengdu 610041, China
[4] Engineering Research Center of Biomass Materials, Ministry of Education, Southwest University of Science and Technology, Mianyang 621010, China

(Received 22 January 2021; revised manuscript received 21 February 2021; accepted manuscript online 25 February 2021)

Lattice defects induced by ion implantation into SiC have been widely investigated in the decades by various techniques. One of the non-destructive techniques suitable to study the lattice defects in SiC is the optical characterization. In this work, confocal Raman scattering spectroscopy and photoluminescence spectrum have been used to study the effects of 134-keV H_2^+ implantation and thermal treatment in the microstructure of 6H-SiC single crystal. The radiation-induced changes in the microstructure were assessed by integrating Raman-scattering peaks intensity and considering the asymmetry of Raman-scattering peaks. The integrated intensities of Raman scattering spectroscopy and photoluminescence spectrum decrease with increasing the fluence. The recovery of the optical intensities depends on the combination of the implantation temperature and the annealing temperature with the thermal treatment from 700 °C to 1100 °C. The different characterizations of Raman scattering spectroscopy and photoluminescence spectrum are compared and discussed in this study.

Keywords: SiC, H_2^+ implantation, Raman scattering spectroscopy, photoluminescence spectrum

PACS: 61.80.–x, 61.80.Jh, 78.30.–j, 78.55.–m **DOI:** 10.1088/1674-1056/abe9a7

1. Introduction

Silicon carbide (SiC), as an important semiconductor material with interesting physical, optical, and electronic properties, is widely used in high-voltage, high-frequency, high-temperature switching devices, as well as in numerous optoelectronic applications.[1] Besides semiconductor industry, SiC can also be used in nuclear power plants because of its low cross-section for neutron capture, excellent chemical, mechanical, and structural stability, as well as low diffusion rate of fission products.[2] In future nuclear reactor, SiC is considered an ideal fuel cladding material for high-temperature gas-cooled fission reactors.[3] Although there are over 200 polytypes of SiC, only face cubic SiC (3C-SiC), considered for nuclear applications and hexagonal 4H-SiC and 6H-SiC having wide-band gap, high-electron mobility, and low-leakage current used in the semiconductor industry, have been extensively investigated so far. To perform selective-area doping in hexagonal SiC, ion implantation has been widely used in the past.

H_2^+ ions-implanted SiC has been extensively investigated to fabricate SiC-on-insulator via the smart-cut technology.[4–10] To elucidate the ion-cut process mechanism and to fabricate advanced electronic devices, it is important to understand the behavior of the implantation-induced defects, their accumulation, and the recovery processes during thermal annealing. Jiang *et al.*[4] use Rutherford backscattering in channeling geometry (RBS/C) to investigate the defect annealing process with annealing temperature in the H_2^+-implanted 6H-SiC. There is no complete recovery even at 800 °C annealing for a fluence of 2.25×10^{16} $H_2^+ \cdot cm^{-2}$ at room temperature implantation. At high fluences of $\geq 7.5 \times 10^{16}$ $H_2^+ \cdot cm^{-2}$, an inner amorphous structure is formed, leading to no significant recovery changes upon 597-°C annealing. Li *et al.*[5] use RBS/C, high-resolution x-ray diffraction and scanning electron microscopy (SEM) to investigate the H_2^+ ions implanted 6H-SiC at room temperatures, 300 °C and 500 °C. The lattice damage decreases gradually with the temperature of the annealing, following the room temperature implantation. However, the reverse annealing effect was observed in H_2^+ ions-implanted 6H-SiC at 300 °C and 500 °C. Transmission electron microscopy (TEM) was used in the study by Zhang and Li[6] to investigate lattice disorder in 6H-SiC implanted by H_2^+ ions to fluences of 0.5×10^{16} $H_2^+ \cdot cm^{-2}$ to 5×10^{16} $H_2^+ \cdot cm^{-2}$

*Project supported by the National Natural Science Foundation of China (Grant No. 12075194), the Sichuan Provincial Science and Technology Program, China (Grant No. 2020ZYD055), and the National Key Research and Development Program of China (Grant No. 2017YFE0301306).

†Corresponding author. E-mail: libingshengmvp@163.com

© 2021 Chinese Physical Society and IOP Publishing Ltd

and annealed at 1100-°C annealing. The size of the observed lattice defects was ranging from 1 nm to 6 nm, with number density in the range of 10^{22} m^{-3} to 10^{23} m^{-3}. Daghbouj *et al.*[7] investigated the blistering phenomenon in H_2^+ ion-implantated 6H-SiC, subjected to high-temperature annealing, by using transmission electron microscopy (TEM) and finite-element method modeling. The blistering efficiency depends on the amount of the formed damage level. Particularly, an implantation-induced amorphous structure can inhibit the occurrence of surface blistering.

It is well known that RBS/C and TEM methods have some drawbacks with respect to particle analysis. Generally, RBS/C analysis uses 2.0-MeV He ions and fabrication of TEM samples is needed due to required transparency to 200-keV or 300-keV electrons. After RBS/C analysis, He ion implantation induces surface color being changed from green to black, due to the increase in the absorption coefficient (not shown).[11] Optical characterization is a good way to avoid sample modification/destruction during measurement. Raman scattering spectrometry technology is widely performed to investigate ions implanted SiC, and it can precisely characterize the evolution of lattice damage with an implantation dose, similar to the result obtained via Rutherford backscattering in channeling geometry.[12–16] Furthermore, Raman scattering spectrometry is sensitive to a low defect concentration via the decrease in Raman scattering intensity, broadening of phonon Raman bands, and frequency shift.[12] In this study, confocal Raman scattering spectroscopy and photoluminescence spectrum are employed to investigate the H_2^+-implanted 6H-SiC followed by thermal annealing. The defect recovery with annealing temperature is characterized by different methods. These two kinds of optical characterizations of lattice damage are compared.

2. Experimental process

Cz-grown N-doped (10^{18} cm^{-3}–10^{19} cm^{-3}), ⟨0001⟩-oriented single crystalline 6H-SiC wafers with 2 inch (1 inch = 2.54 cm) in diameter and 0.35 mm in thickness (supplied by HF-Kejing Inc.), were cut into 1 cm × 1 cm pieces and implanted at room temperature and elevated temperatures (300°C and 500 °C) with 134-keV H_2^+ molecular ions at several fluences ranging from 0.5 × 10^{16} H_2^+·cm^{-2} to 5 × 10^{16} H_2^+·cm^{-2}, respectively. The nominal H concentration depth distribution was obtained from SRIM-2010 using the quick cascade calculation.[17] The mean-projected range R_p was estimated to 393 nm with a straggling ΔR_p of approximately 46 nm (using the density of 3.21 g·cm^{-3} and the threshold displacement energies of 20 eV and 35 eV for C and Si sublattices, respectively). In order to investigate the defect recovery in the sample, isochronal annealing at three different temperatures (700 °C, 900 °C, and 1100 °C) for 15 min in vacuum (∼10^{-3} Pa) was carried out. Surface blisters and exfoliation were observed by scanning electron microscopy when the sample was implanted to a fluence of 1.5×10^{16} H_2·cm^{-2} followed by 1100-°C annealing. An arc-shaped crack located at a depth of approximately 410 nm was formed inside the sample, where is good consistent with the projected range of hydrogen deposition, as shown in Fig. 1. The Raman scattering spectroscopy was performed using a Horiba Join Yvon HR800 spectrometer at room temperature in the backscattering configuration. The excitation wavelength was 532 nm from the Ar^+ laser with a spectral resolution of approximately 0.5 cm^{-1}, and the measurement range was from 100 cm^{-1} to 1000 cm^{-1}. Spectra were recorded with an acquisition time of 30 s. Micro-Raman spectroscopy was employed and the laser spot was approximately 1 μm using a microscopy lens system. The scattered light was detected by a Jobin Yvon T64000 spectrometer with an LN_2 cooled charge-coupled device. The penetration depth of the exciting wavelength is expressed as $d = 1/2\alpha$, where α is the absorption coefficient of the crystalline SiC.[18] The absorption coefficient of single-crystalline 6H-SiC is 115 cm^{-1} at 532 nm based on the UV-visible optical transmittance spectrometer measurement.[12] Therefore, the penetration depth of the exciting wavelength in the single-crystalline 6H-SiC reaches 43 μm, which is far larger than the H_2^+ ion penetration depth. Samples were excited by 325-nm light from a suitably filtered He–Cd laser on the Shimadzu RF-5301 photoluminescence spectroscopy. The measurement was carried out at room temperature (RT), and the exciting wavelength was 340 nm. The measurement range was from 350 nm to 1000 nm.

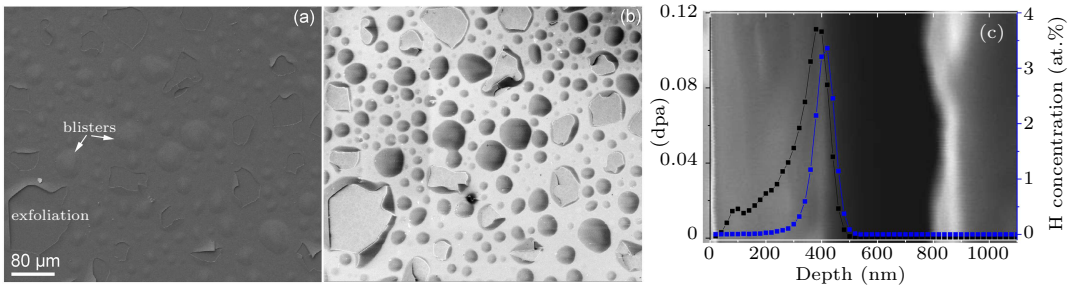


Fig. 1. Cross-sectional scanning electron microscopy, (a) secondary electron image, (b) backscattering electron image of 6H-SiC implanted with 134-keV H_2^+ ions at a fluence of 1.5 × 10^{16} H_2^+·cm^{-2} at 300 °C followed by 1100 °C annealing for 15-min observed by secondary electron (a) and backscattering electron (b), superposed the distribution of damage and hydrogen deposition of the H_2^+-implanted 6H-SiC simulated by SRIM-2010 (c). Blisters and exfoliation are observed in panel (a) and a crack exhibiting black contrast is clearly observed in panel (c).

3. Results and discussion

Figure 2 presents the change of photoluminescence spectra after H_2^+-ion implantation followed by the thermal treatment. An emission peak located at 590 nm was clearly observed. In the present experiment, n-type 6H-SiC due to nitrogen doping was chosen. Meanwhile, using boron as acceptor doping compensates nitrogen doping. Kawai *et al.*[19] argued that the emission peak located at 590 nm is attributed to donor–acceptor pair emission in a SiC crystal. This emission in the range of visible light is convenient for various optical devices, with the intensity of the emission peak being an important parameter in the fabrication process. It is generally regarded that the donor–acceptor pair emission itself is very strong in high-quality SiC.[19] As a result, the emission intensity strongly depends on the quality of the H_2^+ ions-implanted SiC. Figure 2 shows that the location of emission peak did not change significantly after the H_2^+ ion implantation, except for 134-keV H_2^+-implanted SiC at 500 °C after 1100-°C annealing, where large blisters and craters are formed on the surface.[6] This result demonstrates that the donor–acceptor pair emission plays the main role in photoluminescence emission of SiC before and after H_2^+ ion implantation. Moreover, the emission intensity decreased significantly after H_2^+ implantation. The detailed change of the emission intensity *versus* fluence and temperature is presented in Fig. 3.

The Raman spectra of 6H-SiC samples before and after the 134-keV H_2^+-ion implantation to fluences ranging from 0.5×10^{16} $H_2^+ \cdot cm^{-2}$ to 5×10^{16} $H_2^+ \cdot cm^{-2}$ at RT or 2.5×10^{16} $H_2^+ \cdot cm^{-2}$ at RT, 300 °C, and 500 °C, were investigated. In the range of 100 cm^{-1}–1000 cm^{-1}, the group-theoretical analysis indicates that the Raman-active modes of wurtzite structure (C_{6v} symmetry for hexagonal polytypes) are A_1, E_1, and E_2 modes.[20] In addition, A_1 and E_1 phonon modes are split into longitudinal (LO) and transverse (TO) optical modes, respectively. In backscattering configuration, A_1(LO), E_1(LO), and E_2 phonons are observable in Raman spectra.

Figure 3 presents the Raman spectra of 6H-SiC samples, observed Raman peaks located at 144 cm^{-1}/150 cm^{-1}, 266 cm^{-1}, 505 cm^{-1}/513 cm^{-1}, 768 cm^{-1}/790 cm^{-1}, 798 cm^{-1}, 968 cm^{-1} are attributed to E_2(TA), E_2(TA), A_1(LA), E_2(TO), E_1(TO), A_1(LO) phonons, respectively.[21] It can be seen that Raman peaks shift to a lower wavenumber after H_2^+-ion implantation, as shown in Fig. 3(h). The red shift can be attributed to the hydrostatic strain caused by implantation-induced defects.[22] It is interesting to note that one broad band located at 578 cm^{-1} is observed in the H_2^+ ions implanted 6H-SiC after 1100-°C annealing (like 8#SiC), except for 5#SiC. This phonon peak is attributed to the vibration mode of $C_{Si}V_C$ complexes.[23] It is consistent with recent research indicating that many carbon antisite–vacancy pairs formed after 1100-°C annealing measured by transmission electron microscopy and positron annihilation spectrum.[24] It can be seen that the background intensity increased after the H_2^+ ion implantation. This is related to Rayleigh scattering from the implantation-induced damage. However, background intensity increased in the H_2^+ ions implanted 6H-SiC with the thermal treatment, except for 5#SiC. It is associated with the vibrations of silicon and disorder silicon carbide.[21] In addition, the intensities of Raman peaks decreased after H_2^+ ion implantation. The intensities of Raman scattering spectroscopy and photoluminescence spectrum were analyzed and the result is present in Fig. 4.

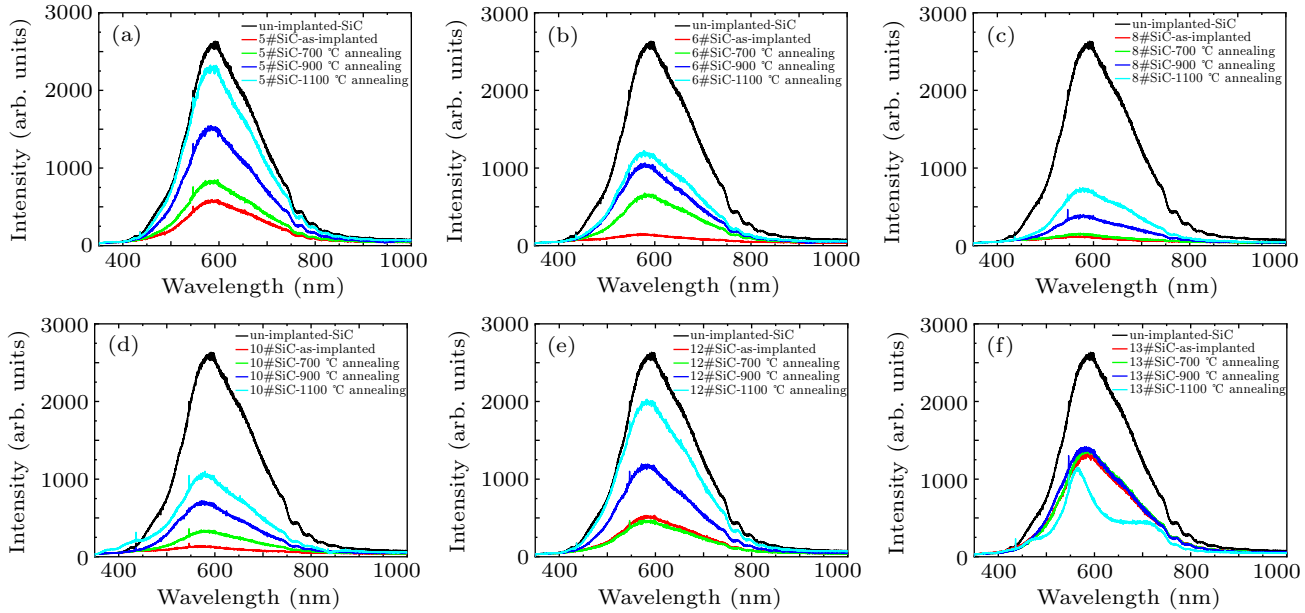


Fig. 2. Photoluminescence spectra from 134-keV H_2^+ ions-implanted 6H-SiC to different fluences after thermal annealing for 15 min. Note that 5#SiC, 6# SiC, 8# SiC, and 10# SiC stand for the implantation fluence of 5×10^{15} $H_2^+ \cdot cm^{-2}$, 1.5×10^{16} $H_2^+ \cdot cm^{-2}$, 5×10^{16} $H_2^+ \cdot cm^{-2}$, and 2.5×10^{16} $H_2^+ \cdot cm^{-2}$ at RT, respectively. 12# SiC and 13# SiC stand for the implantation fluence of 2.5×10^{16} $H_2^+ \cdot cm^{-2}$ at 300 °C and 500 °C, respectively.

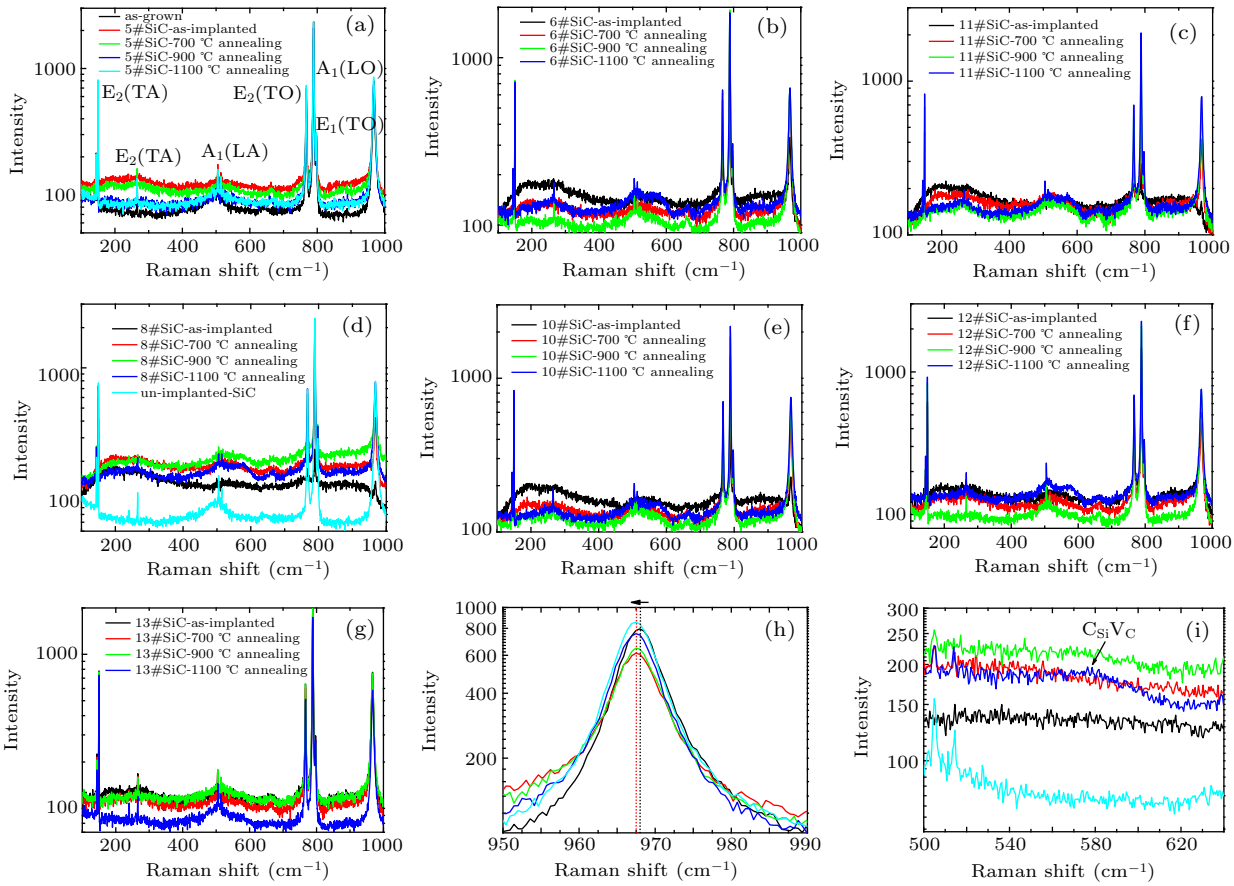


Fig. 3. Raman scattering spectra from 134-keV H_2^+ ions-implanted 6H-SiC to different fluences after thermal annealing for 15 min in vacuum. Note that 11# SiC stands for the implantation fluence of 3.75×10^{15} $H_2^+ \cdot cm^{-2}$ at RT. The left shift of the A_1(LO) peak after H_2^+ ion implantation in the 5# SiC sample before and after annealing is observed in panel (h). (i) The expanded version of Raman spectra in panel (d) shows a broad band at 578 cm^{-1} indicated by a black arrow.

H_2^+-ion implantation can induce dense lattice defects, which destroy lattice structure and decrease the intensity of observed peaks. In general, researchers use the integrated intensity, but not peak intensity, to calculate observed Raman peaks after ion implantation.[11–13] In this study, integrated intensity ΔA of the photoluminescence emission from 400 nm to 850 nm is normalized to the value $\Delta A_{\mathrm{as-grown}}$ of the as-grown sample, and the result is shown in Fig. 4(a). Similarly, integrated intensity ΔA of the A_1(LO) phonon from 940 cm^{-1} to 1000 cm^{-1} is normalized to the value $\Delta A_{\mathrm{as-grown}}$ of the as-grown sample and the result is shown as Fig. 4(b). Compared with the relative intensity between photoluminescence emission and Raman scattering, a similar change trend as a function of the annealing temperature is observed. After 700-°C annealing, the profile slope is positive, except for 12#SiC. Meanwhile, the profile slope is small, which is indicated that the defect recovery is not significant after 700-°C annealing. As for 12#SiC, the relative intensity decreases after 700-°C annealing. It is a reverse annealing phenomenon, which is usually observed by gas ion implantation, such as H^+, He^+. The growing gas bubbles during high-temperature annealing squeeze around C and Si sublattice atoms, which result in punching out self-interstitials, known as loop punching.[25–27] Because the threshold temperature for Si vacancy migration in SiC is above 900 °C and C vacancy needs higher temperature,[28] it is reasonable to regard that bubbles cannot be formed after 700-°C annealing. The possible reason is the migration and accumulation of interstitials into interstitial-type clusters after 700-°C annealing. The intensity of the photoluminescence emission depends on the donor–acceptor pair number, while the intensity of the Raman scatting depends on the optical absorption coefficient. The decrease in relative intensity indicates the reduction in the donor–acceptor pair number and the increase in the optical absorption coefficient via these interstitial-type clusters.[12,16,21] With increasing annealing temperature from 700 °C to 900 °C, all profiles have positive slopes, indicating the defect recovery after 900-°C annealing. With increasing annealing temperature from 900 °C to 1100 °C, the profile slope is positive, except for 13#SiC. It can be attributed to the growth of vacancy-type defects, like micro-cracks after 1100-°C annealing. The microstructure in the H_2^+ ions-implanted 6H-SiC after 1100-°C annealing is reported in our recent article.[6] The difference between the two methods is the range of the relative intensity. In the whole, the relative intensity of the photoluminescence emission is smaller than that of Raman scattering, which indicates that lattice defects have more influence on the number

of donor–acceptor pair than the optical absorption coefficient. As for an important semiconductor and optical material, fabrication of p–n junction via ion-doping into SiC, implantation-induced lattice defects should be taken into consideration.

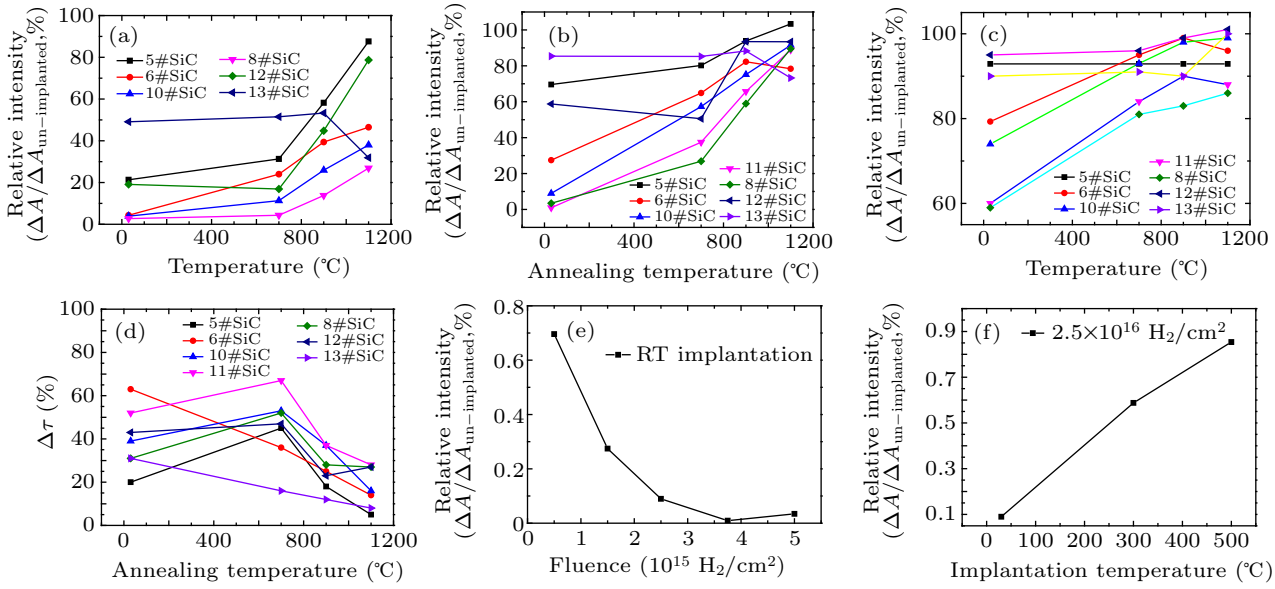


Fig. 4. (a) Relative integrated intensity of the photoluminescence emission after H_2^+-ion implantation before and after annealing, (b) relative integrated intensity of the A_1(LO) phonon at 968 cm^{-1} after H_2^+-ion implantation before and after annealing, (c) relative intensity of the ratio of E_2(TO) to A_1(LO) after H_2^+-ion implantation before and after annealing, (d) asymmetry of the A_1(LO) phonon after H_2^+-ion implantation before and after annealing, (e) relative integrated intensity of the A_1(LO) phonon at 968 cm^{-1} after H_2^+-ion implantation to different fluences at RT, (f) relative integrated intensity of the A_1(LO) phonon at 968 cm^{-1} after H_2^+-ion implantation to the same fluence at RT, 300 °C, and 500 °C.

Besides the lattice defects, the focused condition also affects the Raman scattering intensity. In order to reduce the influence of the focused condition on the Raman peaks, the peak intensity of E_2(TO) phonon divides by A_1(LO) phonon ($\Delta h = h_{\rm E2}/h_{\rm A1}$, and relative intensity is $\Delta h/\Delta h_{\rm as-grown}$) is chosen to calculate the defect recovery after annealing. One can see a sharp difference between $\Delta A/\Delta A_{\rm as-grown}$ and $\Delta h/\Delta h_{\rm as-grown}$. First, the relative intensity is different. The integrated intensity is near zero for 11#SiC and 8#SiC, while the peak intensity of E_2(TO) phonon divides by A_1(LO) phonon is near 60% for the same sample. The microstructure shows an amorphous layer formed in the 11#SiC and 8#SiC, resulting in the disappearance of characteristic SiC Raman scattering peaks. Secondly, the change of the profile slope is different. For example, there is no change basically with annealing temperature for the 5#SiC via the calculation of $\Delta h/\Delta h_{\rm as-grown}$, while the relative intensity increased with annealing temperature via the calculation of $\Delta A/\Delta A_{\rm as-grown}$. Generally, the as-implanted sample has the largest concentration of survival defects, while Frenkel pairs migrate and recombine each other to reduce the survival defects after 700-°C annealing. As for the 5#SiC, lattice disorder recovery after the thermal treatment is precisely characterized by $\Delta A/\Delta A_{\rm as-grown}$, but not $\Delta h/\Delta h_{\rm as-grown}$. In addition, the $\Delta A/\Delta A_{\rm as-grown}$ decreases after 1100-°C annealing for the 13#SiC. On the contrary, the $\Delta h/\Delta h_{\rm as-grown}$ increases. Our previous result shows an obvious micro-crack formed in the 13#SiC after 1100-°C annealing. There are dense frank loops formed around the micro-crack.[6] These frank loops and some undiscovered defects induce the decrease in the Raman scattering intensity and the increase in the asymmetry of A_1(LO) phonon. The asymmetry of A_1(LO) phonon cannot be characterized by $\Delta h/\Delta h_{\rm as-grown}$. Therefore, using the peak intensity of E_2(TO) phonon divides by A_1(LO) phonon is not accurate for characterizing the lattice disorder.

To investigate the asymmetry of A_1(LO) phonon, the intensity of the asymmetry is described by $\Delta\tau = (I_{\rm left} - I_{\rm right})/I_{\rm right}$, where I is the intensity of Raman scattering baseline. Based on experimental results, $I_{\rm right}$ at $x = 1000$ cm^{-1}, and $I_{\rm left}$ at $x = 936$ cm^{-1} (the A_1(LO) peak located at 968 cm^{-1}) are observed and the calculation result is shown in Fig. 4(d). It can be seen that there is a linear change with annealing temperature for the 6#SiC and 13#SiC, while $\Delta\tau$ increases initially and then decreases with the annealing temperature for the other samples. It is a surprise that the relative intensity of 6#SiC is the largest compared with other as-implanted samples. Because 6#SiC is implanted with a fluence of 1.5×10^{16} $H_2^+\cdot$cm^{-2}, the implantation-induced lattice defects are less than the case of 10#SiC. The asymmetric broadening of the A_1(LO) phonon can be accounted for as a "spatial correlation" model that implantation-induced defects can induce q-vector relaxation.[29] The increase in defect density induces an asymmetry of A_1(LO) phonon with an obvious tail in the range of 900 cm^{-1}–967 cm^{-1}. Two potential reasons are used to explain why the number of $\Delta\tau$ for the 6#SiC is the largest. The first reason is the growth of the optical absorption coefficient with increasing fluence. Ra-

man scattering intensity decreases with increasing optical absorption coefficient.[12,16,21] Meanwhile, the decrease in I_{right} is faster than that of I_{left}. The Raman scatting results show that the intensity of Raman scattering baseline does not increase with growing lattice disorder. The second reason is that the lattice defects enhance Raman activation, such as a peak located at 935 cm^{-1}–940 cm^{-1} due to the vibration of disordered SiC.[21] Based on the above analysis, using $(I_{\text{left}} - I_{\text{right}})/I_{\text{right}}$ cannot precisely characterize the asymmetry of A_1(LO) phonon.

Figure 4(e) shows the relative integrated intensity of the sample implanted at RT without annealing. It can be clearly seen that the curve exhibits an exponential decrease with increasing the fluence. It is consistent with previous research that disorder accumulation can be explained by direct impact/defect simulation model or multi-step transformation process.[30,31] Figure 4(f) shows the relative integrated intensity of the sample implanted at elevated temperature without annealing. It exhibits a linear growth of intensity with increasing the implantation temperature. This result indicates the recovery of the same type of lattice defects during implantation at 300 °C and 500 °C, where only interstitial-type defects can migrate.

4. Conclusion

In this study, the formation and evolution of lattice disorder in the H_2^+ ions-implanted 6H-SiC are investigated by using Raman scattering spectroscopy and photoluminescence spectrum. The influence of lattice disorder on the intensity of observed peaks is discussed in details. The lattice disorder has a more pronounced effect on the intensity of photoluminescence emission, compared to the intensity change measured by Raman scattering. This conclusion demonstrates that the number of donor–acceptor pair decreases significantly when SiC crystal contains lattice defects. It is recommended to pay particular attention to lattice damage in performing selective-area doping technique via ion implantation. It is the integrated intensity of Raman scattering, but not the peak intensity of E_2(TO) phonon divided by A_1(LO) phonon and $(I_{\text{left}} - I_{\text{right}})/I_{\text{right}}$, that can precisely characterize the evolution of lattice disorder in SiC.

Acknowledgement

The authors appreciate the Laboratory of 320-kV High-Voltage Platform in the Institute of Modern Physics, Chinese Academy of Sciences for the helium implantation. We would like to thank Dr. Vladimir Krsjak for the writing revision.

References

[1] Park C H, Cheong B H, Lee K H and Chang K J 1994 *Phys. Rev. B* **49** 4485
[2] Snead L L, Nozawa T, Katoh Y, Byun T S, Kondo S and Petti D A 2007 *J. Nucl. Mater.* **371** 329
[3] Tan L, Allen T R, Hunn J D and Miller J H 2008 *J. Nucl. Mater.* **372** 400
[4] Jiang W, Weber W J, Thevuthasan S and Grotzschel R 2000 *Nucl. Instrum. Method B* **166–167** 374
[5] Li B S, Wang Z G and Jin Y F 2013 *Nucl. Instrun. Method B* **316** 239
[6] Zhang L and Li B S 2017 *Physica B* **508** 104
[7] Daghbouj N, Li B S, Callisti M, Sen H S, Jin J, Ou X, Karlik M and Polcar T 2020 *Acta Mater.* **188** 609
[8] Daghbouj N and Li B S, Karlik M and Delcemy A 2019 *Appl. Surf. Sci.* **466** 141
[9] Gregory R B, Wetteroth T A, Wilson S R, Holland O W and Thomas D K 1999 *Appl. Phys. Lett.* **75** 2623
[10] Jia Q, Huang K, You T G, Yi A L, Lin J J, Zhang S B, Zhou M, Zhang B, Yu W J, Ou X and Wang X 2018 *Appl. Phys. Lett.* **112** 192102
[11] Zhang H H, Zhang C H, Li B S, Zhou L H, Yang Y T and Fu Y C 2009 *Acta Phys. Sin.* **58** 3302 (in Chinese)
[12] Li B S, Zhang C H, Zhang H H, Shibayama T and Yang Y T 2011 *Vacuum* **86** 452
[13] Du Y Y, Li B S, Wang Z G, Sun J R, Yao C F, Pang L L, Zhu Y B, Cui M H, Zhang H P, Li Y F, Wang J, Zhu H P, Song P and Wang D 2014 *Acta Phys. Sin.* **63** 216101 (in Chinese)
[14] Li B S, Liu H P, Kang L, Zhang T M, Xu L J and Xiong An L 2019 *J. Eur. Cer. Soc.* **39** 4307
[15] Zhang L M, Jiang W L, Pan C L, Fadanelli R C, Ai W S, Chen L and Wang T S 2019 *J. Raman Spectroscopy* **50** 1197
[16] Heliou R, Brebner J L and Roorda S 2001 *Nucl. Instrum. Method B* **175–177** 268
[17] http://www.srim.org
[18] Harima H 2006 *Microelectronic Eng.* **83** 126
[19] Kawai Y, Maeda T, Nakamura Y, Sakurai Y, Iwaya M, Kamiyama S, Amano H, Akasaki I, Yochimoto M, Furusho T, Kinoshita H and Shiomi H 2006 *Mater. Sci. Forum* **527–529** 263
[20] Nakashima S and Harima H 1997 *Phys. Stat. Sol. (a)* **162** 39
[21] Sorieul S, Costantini J M, Gosmain L, Thome L and Grob J J 2006 *J. Phys.: Condens. Matter* **18** 5235
[22] Huang X, Ninio F, Brown L J and Prawer S 1995 *J. Appl. Phys.* **77** 5910
[23] Wang P F, Huang L, Zhu W and Ruan Y F 2012 *Solid State Commun.* **152** 887
[24] Li B S, Krsjak V, Degmova J, Wang Z G, Shen T L, Li H, Sojak S, Slugen V and Kawasuso A 2020 *J. Nucl. Mater.* **535** 152180
[25] Liu Y Z, Li B S and Zhang L 2017 *Chin. Phys. Lett.* **34** 052801
[26] Han W T and Li B S 2018 *J. Nucl. Mater.* **504** 161
[27] Liu H P, L i J Y and Li B S 2018 *Chin. Phys. Lett.* **35** 096103
[28] Gao F, Weber W J, Posselt M and Belko V 2004 *Phys. Rev. B* **69** 245205
[29] Richter H, Wang Z P and Ley L 1981 *Solid State Commun.* **39** 625
[30] Zhang Y, Weber W J, Jiang W, Hallen A and Possnert G 2002 *J. Appl. Phys.* **91** 6388
[31] Jagielski J and Thome L 2009 *Appl. Phys. A* **97** 147